Here, the Young's modulus of human radial artery was compromised to be compared with that of canine aorta as the representative of canine arteries due to limitation of available data, though it should normally be compared with that of canine carotid artery or femoral artery with which the tube law was presented. The Young's modulus correlates with the gradient of ϕ at $A/A_0 = 1.0$, and is larger in peripheral arteries than central arteries[14]. The determined parameters, however, were used as the reference values and contribution of the Young's modulus to the pressure pulse waves was discussed in section 3.2.

The forth term of the right-hand side of Eq. (4) is viscous resistance to the change in cross-sectional area of the artery by the surrounding tissue. The damping coefficient γ against the change in the cross-sectional area of the artery was obtained as 2.5×10^8 Pa·s/m^2 from experimental data of loss of elastic coefficient of the canine artery[20]. However, since this value was so big for stable computation that we compromised by giving the largest coefficient $\gamma = 2.5\times10^7$ Pa·s/m^2 among the range of stable computation. The microvasculature was approximated by a linear resistance with the resistance coefficient R_m of 4.3×10^9 Pa·s/m^3, and the venous system was approximated by the Windkessel model with the resistance coefficient R_v of 8.3×10^8 Pa·s/m^3 and capacitance C_v of 1.95×10^{-9} m^3/Pa[11].

We also have to take into consideration the transfer characteristics of the subcutaneous tissue between the pressure sensor and the arterial vessel wall to reproduce the indentation experiment explained in section 2.1. The relationship between the compression of the tissue by the pressure sensor and vessel wall, and repulsion pressure of the tissue to artery P_e is given as

$$P_e = a(Y + dy_{av})^2, \tag{6}$$

where $a = 10.0\times10^8$ Pa/m^2 is the coefficient of the subcutaneous tissue model[11], and dy_{av} is the mean value of dy under the center of the sensor as shown in Fig. 4, where dy is displacement of the artery wall from its steady state y_0. Here, both Y and dy_{av} are positive in the direction of compression of the tissue, and pressure detected by the sensor P_o equals the external pressure of the artery P_e according to the principle of reaction.

Numerical simulation was performed by the 4th-order Runge-Kutta method with the time step of $\Delta t = 10^{-7}$ s to solve pulsatile blood flow and deformation of blood vessel simultaneously. Here, as for the supply pressure, the waveform shown in Fig. 5 was determined from the measured data at the brachial artery[21] as the mean value $P_{sav} = 13.3$ kPa (100 mmHg) and amplitude $\Delta P_s = 5.5$ kPa (41.25 mmHg)[11]. The artery was divided into 284 cells with non-uniform meshing so that the mesh under the pressure sensor was accumulated to 16 cells[11].

3. Results and Discussion

In the following sections, the indentation experiment introduced in section 2.1 was numerically reproduced with the mathematical model to investigate the contribution of the supply pressure of the blood and the tube law of the artery to the changes in mean value P_{oav} and amplitude ΔP_o of the pressure P_o detected by the sensor with the indentation steps. Lastly to verify their contribution to the pressure pulse waves detected by the sensor, it was examined to reproduce the pressure pulse waves measured in the indentation experiment with the mathematical model by adjusting the parameters.

3.1 Effect of Supply Pressure

In this section, the contribution of the supply pressure P_s at the upstream end of the collapsible tube to P_{oav} and ΔP_o was examined numerically. For this purpose, mean value P_{sav} and amplitude of pulsation ΔP_s of P_s were changed from the original values, $P_{sav} = 13.3$ kPa and $\Delta P_s = 5.5$ kPa, keeping the waveform shown in Fig. 5. In the classification of blood pressure range put forwarded by the Japan Society of Hypertension, normal ranges of the systolic pressure, diastolic pressure and amplitude of the pulsation are less than 140 mmHg,

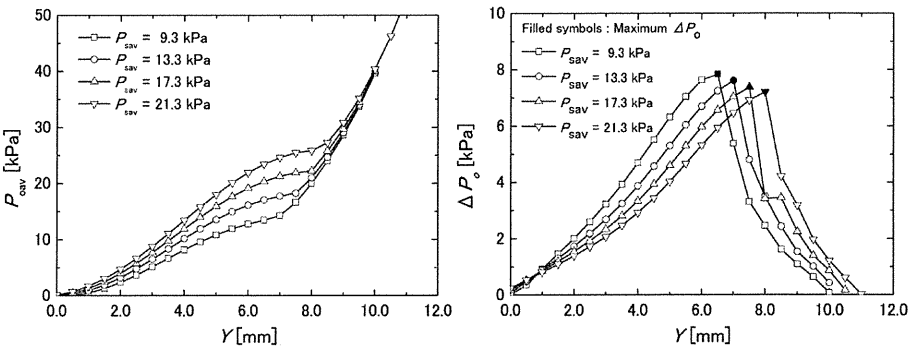

(a) Mean pressure P_{oav}. (b) Amplitude of pulsation ΔP_o.

Fig. 6 Numerical reproduction of indentation experiment with four mean supply pressure P_{sav}.

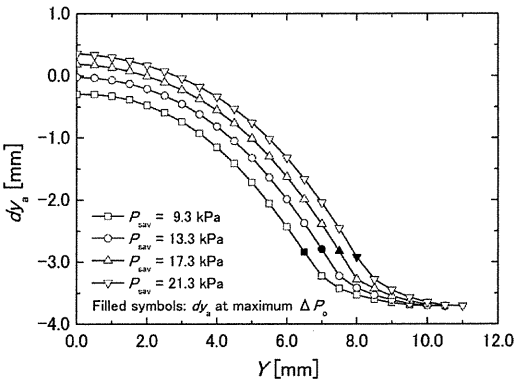

Fig. 7 Relationship between indentation Y and time-averaged displacement of vessel wall under the center of the sensor dy_a.

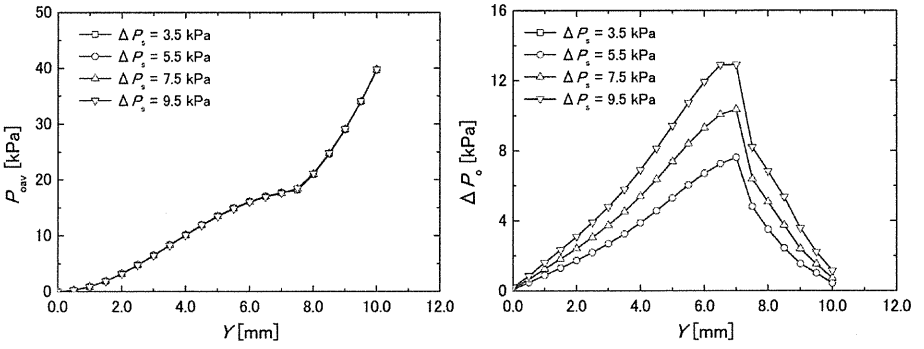

(a) Mean pressure P_{oav}. (b) Amplitude of pulsation ΔP_o.

Fig. 8 Numerical reproduction of indentation experiment with four amplitude of supply pressure ΔP_s.

less than 90 mmHg, and 30 to 50 mmHg, respectively[22]. Therefore, mean pressure of 13.3 kPa (100 mmHg) and amplitude of 5.5 kPa (41.3 mmHg) is in the normal range, respectively.

First, P_{sav} was chosen from among 9.3, 13.3, 17.3 and 21.3 kPa while keeping the amplitude ΔP_s = 5.5 kPa. Figures 6(a) and 6(b) show the numerically obtained relationship between Y and P_{oav}, and Y and ΔP_o, respectively. In Fig. 6(a), P_{oav} is higher for high P_{sav} in the range $Y < 8.0$ mm. This is explained as follows: Figure 7 shows the relationship between Y and time-averaged displacement of the vessel wall under the center of the sensor dy_a. We can say from this figure that dy_a increases with the increase in the inner pressure P_{sav} at a fixed Y to compress the subcutaneous tissue from inside the arm by the vessel, and thus,

P_{oav}, which equals the time-averaged value of P_e in Eq. (6), increases with the increase in P_{sav} since dy_{av} increases with the increase in dy_a. On the contrary, the difference in P_{oav} between high and low P_{sav} becomes small in the range of $Y \geq 8.0$ mm, and the lines in Fig. 6(a) follow the tube law in negative ϕ.

In Fig. 6(b), Y which gives the maximum ΔP_o increases with the increase in P_{sav}. This is explained as follows: Filled symbols in Fig. 7 correlate with those in Fig. 6(b). In Fig. 7, dy_a which gives the maximum ΔP_o is almost constant and A/A_0 was about 0.15 independent of P_{sav} while dy_a at $Y = 0$ mm increases with P_{sav}. Therefore, displacement of the sensor Y to press the vessel wall down to this point increases with the increase in P_{sav}. Here, the peak value of ΔP_o slightly decreases with the increase in Y. This implies that, though the precise mechanism is unknown, the peak value decreases as the subcutaneous tissue is compressed.

Next, ΔP_s was chosen from among 3.5, 5.5, 7.5 and 9.5 kPa while keeping $P_{sav} = 13.3$ kPa. Figures 8(a) and 8(b) show the numerically obtained relationship between Y and P_{oav}, and Y and ΔP_o, respectively. In Fig. 8(a), P_{oav} is not influenced by ΔP_s. This is because that, since ϕ correlates with the supply pressure P_s, mean value of A/A_0 at each Y does not change with ΔP_s so far as P_{sav} is fixed. On the contrary, as shown in Fig. 8(b), ΔP_o increases with the increase in ΔP_s, and the value of ΔP_o at each Y is nearly proportional to ΔP_s. This is because that amplitude of A/A_0 becomes large with the increase in ΔP_s.

Here, it is generally said to be low blood pressure when systolic blood pressure is less than 100 mmHg, and it is said to be high blood pressure when systolic and diastolic blood pressures are 140 mmHg or more and 90 mmHg or more, respectively[22]. When $P_{sav} = 9.3$ kPa, systolic blood pressure at $\Delta P_s = 3.5$ kPa is 87 mmHg and is determined to be in the low blood pressure. When $P_{sav} = 21.3$ kPa, systolic and diastolic blood pressures at $\Delta P_s = 11.5$ kPa are 207 mmHg and 136 mmHg, respectively, and it is classified to be in the serious high blood pressure in which systolic and diastolic blood pressures are 180 mmHg or more and 110 mmHg or more, respectively. Therefore, the combination of P_{sav} and ΔP_s covers from the low blood pressure to the high blood pressure.

3.2 Effect of Tube Law of Artery

Although the tube law is an important parameter which expresses the stiffness of the arterial vessel wall, there have been few attempts to observe it directly. Many research studies have been performed to observe the relationship between transmural pressure and the diameter of an artery to predict the physical characteristics of the vessel wall, and a non-dimensional parameter named the stiffness parameter β has been introduced[23]. The relationship between inner pressure P and radius R of an artery under the physiological condition is expressed as

$$\ln\left(\frac{P}{P_b}\right) = \beta\left(\frac{R}{R_b} - 1\right), \tag{7}$$

where P_b is an arbitrary inner pressure (generally $P_b = 13.3$ kPa), and R_b is the radius at $P = P_b$. Assuming that the cross section of the artery is a circle under the physiological conditions, we can obtain β from the tube law as

$$\beta = \frac{2}{P_b} \frac{dP}{d(A/A_0)}\bigg|_{A/A_0=1}. \tag{8}$$

The stiffness parameter of human arteries is known to increase with aging or progression of diseases[23]. In this section, the influence of the stiffness of the artery on the measured pressure pulse waves is examined numerically. For this purpose, a parameter of the tube law n_1 was chosen from among 2, 3, 6 and 12, taking into consideration the stiffness parameter obtained with the carotid and femoral arteries of human[24]. The correspondence of n_1 and β of the above-mentioned n_1 is shown in Table 1 together with that of the original $n_1 = 5$. The n_1 influences the gradient of the tube law at $A/A_0 = 1$, the

Table 1 Correspondence table between parameter n_1 of tube law and stiffness parameter β.

n_1	2	3	5	6	12
β	4.0	5.9	9.7	11.6	23.0

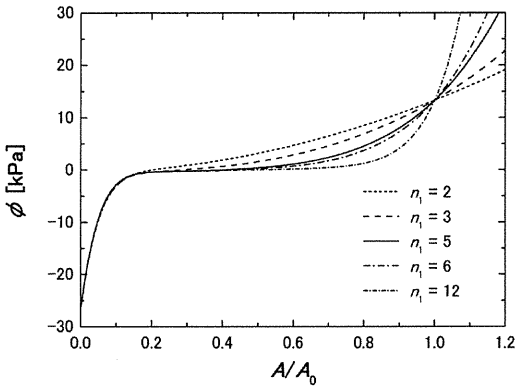

Fig. 9 Variation of tube law by n_1.

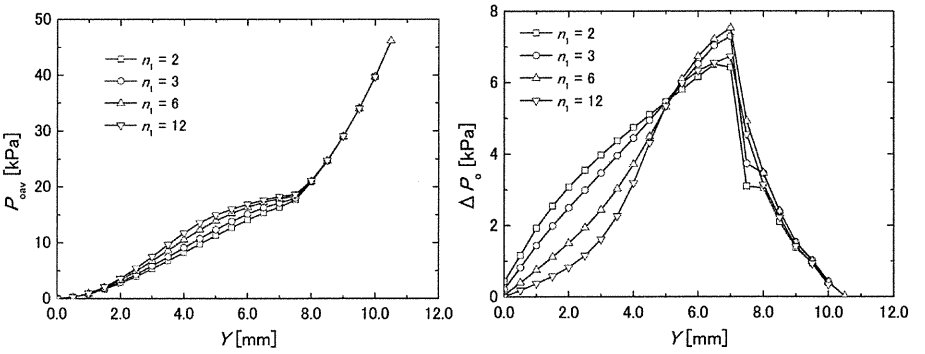

(a) Mean pressure P_{oav}. (b) Amplitude of pulsation ΔP_o.

Fig. 10 Numerical reproduction of indentation experiment with four tube laws.

artery in the physiological range of the transmural pressure, 10.5 kPa < ϕ < 16.0 kPa, becoming hard as n_1 increases, as shown in Fig. 9. Here, the authors compromised by giving almost the same tube law in the range of ϕ < 0.0 kPa (A/A_0 < 0.2) because they have neither measurement data of the tube law out of the range of blood pressure nor knowledge of the influence of such factors as aging or arteriosclerosis on the tube law. The gradient of the tube law is decreased as the increase in n_1 in the positive range of small transmural pressure ϕ. This represents the cross section A decreases drastically with a small decrease in ϕ.

Figures 10(a) and 10(b) show the numerically obtained relationship between Y and P_{oav}, and Y and ΔP_o, respectively, for the four variations of n_1. Here it was confirmed that the displacement of the artery under the center of the pressure sensor $|dy_a|$ was smaller for large n_1 in the range of Y < 8 mm. Since dy_a is negative in the direction of indentation, measured pressure P_o becomes larger for large n_1 as understood from Eq. (6). Therefore, P_{oav} is large for large n_1, as shown in Fig. 10(a) in the range of Y < 8 mm, and thus, it can be said that a soft artery reduces the measured mean pressure. On the contrary, P_{oav} in the range of $Y \geq 8$ mm is almost the same independent of n_1 and follows the tube law in the negative ϕ region of A/A_0 < 0.15.

The profile of the relationship between Y and ΔP_o in Fig. 10(b) drastically changes in the range of $Y \leq 5$ mm, i.e., it is convex-up for small n_1 but becomes convex-down with the

Table 2 Parameters which best fit the experimental data.

a [Pa/m^2]	P_{sav} [kPa]	ΔP_s [kPa]	n_1
11.0×10^8	8.3	4.5	8

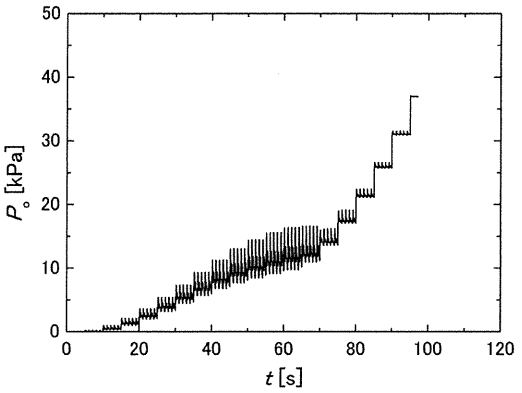

Fig. 11 Pressure pulse waves obtained by numerical simulation with the parameters shown in Table 2.

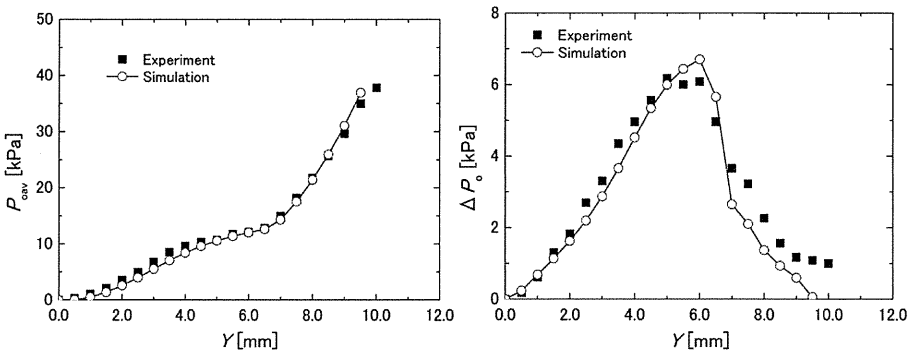

(a) Mean pressure P_{oav}. (b) Amplitude of pulsation ΔP_o.

Fig. 12 Comparison of numerical result with experimental data.

increase in n_1. This is because, as seen in Fig. 9, in the range of small Y, change in the cross-sectional area for a certain amplitude of ϕ is small for large n_1 owing to difference in the gradient of ϕ around $A/A_0 = 1$. This difference in the profile can be an index to predict the stiffness parameter. Here, the reason for the kink at $Y = 7.5$ mm is unknown.

3.3 Reproduction of Experimental Data

To verify the contribution of the parameters of the subcutaneous tissue model[11], the supply pressure and the tube law to the changes in P_{oav} and ΔP_o, numerical reproduction of the experimentally obtained pressure pulse waves shown in Fig. 2 was examined. The parameters determined to best fit the experimental result are listed in Table 2, and the resultant numerically obtained pressure pulse waves are shown in Fig. 11. The relationship between Y and P_{oav}, and Y and ΔP_o are shown in Fig. 12(a) and 12(b), respectively. Both P_{oav} and ΔP_o show better agreement to the experimental data than the former result[11]. In Fig. 12(b), however, the discrepancy in ΔP_o in the range of $Y \geq 7$ mm is relatively larger than that in the range of $Y < 7$ mm. This is considered to be because pressure pulsation propagates backward to the collapsed radial artery via the ulnar artery and the palmar arch in addition to arbitrary determination of the tube law in the negative transmural pressure range.

4. Conclusions

A simple mathematical model of one-dimensional blood flow in the artery of an arm and the subcutaneous tissue on the radial artery was developed, while in a previous study, an experimental setup to press a pressure sensor against the radial artery at the wrist was designed for the purpose of collecting scientific evidence for pulse diagnosis[11]. An experiment to indent the radial artery in a stepwise manner by the pressure sensor was performed to measure the change in the pressure pulse waves with the indentation steps. The experiment was then numerically reproduced with a mathematical model, suggesting that the mathematical model has a potential to quantitatively reproduce the pulse diagnosis.

In the present study, contributions of parameters of the supply pressure of blood and the tube law of the artery to the changes in the mean value and amplitude of the pressure pulse waves when the pressure sensor was pressed down on the radial artery were examined using the mathematical model. Obtained results summarized in terms of the displacement Y of the sensor are enumerated as follows: (1) The mean pressure increased with the increase in mean supply pressure. However, it followed the tube law in the negative transmural pressure range after the artery was nearly collapsed by the sensor. The Y which gave the maximum amplitude of the pulsation increased and the peak value slightly decreased with the increase in the mean supply pressure. (2) The Y which gave the maximum amplitude of the pulsation did not change, but the amplitude increased nearly in proportion to the amplitude of the supply pressure. (3) The profile of the amplitude of pulsation in the range of $Y \leq 5$ mm drastically changed from convex-up to convex-down with the increase in n_1 of the tube law. This change in the profile is a possible index to predict the stiffness parameter of the artery.

It was examined to reproduce the pressure pulse waves measured in the indentation experiment with the mathematical model by adjusting parameters taking into consideration these results. It was suggested that pressure pulsation propagates backward to the collapsed radial artery via the ulnar artery and the palmar arch. Therefore, the authors are planning to extend the blood circulation system of an arm to take into consideration the blood perfusion through the ulnar artery.

Acknowledgements

A part of this research was performed with the support of the Sendai Area Knowledge Cluster Initiative (Stage II). The authors appreciate the helpful suggestions of Professor Shin-ichi Nitta, Associate Professor Hiroshi Kawada, Senior Assistant Professor Mitsuya Maruyama and Assistant Professor Satoshi Konno of Institute of Development, Aging and Cancer, Tohoku University, Dr. Takashi Seki of Tohoku University Hospital, and Associate Professor Makoto Ohta of Institute of Fluid Science, Tohoku University.

References

(1) Shirota, F., Mitsufuji, H., and Igarashi, H., Scientific Verification of Oriental Diagnoses, *Kampo Med.*, Vol. 22 (1972), pp. 201-209. (in Japanese)

(2) Takashima, M., Nagaya, K., Kikuna, T. and Matsuya, K., Development of new apparatus for oriental pulse diagnosis, *Kampo Med.*, Vol. 47 (1997), pp. 635-643. (in Japanese)

(3) Fujita, R., The study of pulse diagnosis (18th. Report) – improved photoelectroplethysmograph – (2nd. report), *Kampo Med.*, Vol. 28 (1977), pp. 81-84. (in Japanese)

(4) Onaka, M., Objectification of the pulse diagnosis by arterial tonometry, *Oriental Med. Pain Clinic*, Vol. 31 (2001), pp. 34-40. (in Japanese)

(5) Uebaba, K., O'rourke, M.F., Xu, F., Ishiyama, H., Amano, K. and Kasahara, H., Radial artery pulse wave analysis in assessment of cardiac function – Value of traditional pulse diagnosis –, *Eastern Med.*, Vol. 17, No. 2 (2001), pp. 1-13.

(6) Konno, S., Maruyama, M., Nitta, S., Takashima, M., Shiraishi, Y., Yambe, T., Ohta, M., Ryu, R., Narumi, K., Shirai, A., Hayase, T., and Yoshizawa, M., Effect of the blood flow of ulnar artery on radial artery pulse wave, *Transactions of the Japanese Society for Medical and Biological Engineering*, Vol. 44, Suppl. 1 (2006), pp. 592. (in Japanese)
(7) Olufsen, M.S., Structured tree outflow condition for blood flow in larger systemic arteries, *Am. J. Physiol. Heart Circ. Physiol.*, Vol. 276 (1999), pp. 257-268.
(8) Sherwin, S.J., Franke, V., Peiro, J. and Parker, K., One-dimensional modeling of a vascular network in space-time variables, *J. Eng. Math.*, Vol. 47 (2003), pp. 217-250.
(9) Vignon, I.E. and Taylor, C.A., Outflow boundary conditions for one-dimensional finite element modeling of blood flow and pressure waves in arteries, *Wave Motion*, Vol. 39 (2004), pp. 361-374.
(10) Alastruey, J., Parker, K.H., and Peiró, J., Analysing the pattern of pulse waves in arterial networks: a time-domain study, *J. Eng. Math.*, Vol. 64 (2009), pp. 331-351.
(11) Narumi, K., Nakanishi, T., Shirai, A., and Hayase, T., Development of One-Dimensional Mathematical Model for Validation of Pulse Diagnosis, *Trans. JSME*, Ser. B, Vol. 74, No. 737 (2008), pp.142-148. (in Japanese)
(12) Ohnaka, M., Investigation of Objective Evaluation of Pulse Diagnosis, *Oriental Medicine and The Pain Clinic*, Vol. 31 (2001), pp. 34-40. (in Japanese)
(13) Hayashi, S., Hayase, T., Shirai, A., and Maruyama, M., Numerical Simulation of Noninvasive Blood Pressure Measurement, *Trans. ASME, J. Biomech. Eng.*, Vol. 128 (2006), pp. 680-687.
(14) Wang, J.J., and Parker, K.H., Wave propagation in a model of the arterial circulation, *J. Biomech.*, Vol. 37 (2004), pp. 457-470.
(15) Hershey, D., and Smolin, R., Linear regime transition for blood flow in tubes, *Biorheology*, Vol. 4 (1966), pp. 61-67.
(16) Okino, H., Sugawara, M., and Matsuo, H. ed., *Dynamics and Fundamental Measurement of Cardiovascular System*, Kodan-sha (1980), pp. 125-132. (in Japanese)
(17) Nikurades, J., Gesetzmässigkeit der tuburenten Strömung in glatten Rohren, *Forsch. Abr. Ing. –Wes.*, 356 (1932).
(18) Shimizu, M. and Ryumae, S., Model of Arterial Volume Change under the Cuff during Blood Pressure Measurement, *Japanese Journal of Medical Electronics and Biological Engineering*, Vol. 30, No. 4 (1992), pp. 267-275. (in Japanese)
(19) Oka, S., *Biorheology*, Syokabo Publishing Co. Ltd. (1984). (in Japanese)
(20) Bergel, D.H., The Dynamic Elastic Properties of Arterial Wall, *J. Physiol.*, Vol. 156 (1961), pp. 458-469.
(21) Yoshimura, M., Mishima, Y., Hattori, K., and Maeda, K. ed., *Clinical Pulse Wave Decipherment Course I*, Kanehara & Co., Ltd. (1994). (in Japanese)
(22) Ozawa, T., Editorial: Clinical measurement of pulse pressure, *Arterial Stiffness No. 8*, Medical View Co. Ltd. (2005). (in Japanese)
(23) Hayashi, K., *Biomechanics*, Corona Publishing Co. Ltd. (2000). (in Japanese)
(24) Kawasaki, T., Sasayama, S., Yagi, S., Asakawa, T., and Hirai, T., Non-invasive assessment of the age related changes in stiffness of major branches of the human arteries, *Cardiovasc. Res.*, Vol. 21 (1987), pp. 678-687.

Expert Opinion

informa
healthcare

Positron emission tomography evaluation of sedative properties of antihistamines

Kazuhiko Yanai†, Dongying Zhang, Manabu Tashiro, Takeo Yoshikawa, Fumito Naganuma, Ryuichi Harada, Tadaho Nakamura, Katsuhiko Shibuya & Nobuyuki Okamura
†*Tohoku University Graduate School of Medicine, Department of Pharmacology, Sendai, Japan*

Introduction: H_1 antihistamines are often used in the medication for allergic diseases, coughs and colds, and insomnia, with or without prescription, even though their sedative properties are a potentially dangerous unwanted side effect that is not properly recognized. These sedative properties have been evaluated using the incidence of subjective sleepiness, objective cognitive and psychomotor functions, and positron emission tomography (PET) measurement of H_1 receptor occupancy.

Areas covered: This article reviews the current updated literature on the sedative properties of antihistamines examined by PET measurement of H_1 receptor occupancy.

Expert opinion: The use of PET to examine antihistamine penetration in the human brain in relation to psychometric and other functional measures of CNS effects is a major breakthrough and provides a new standard by which the functional CNS effects of antihistamines can be related directly to H_1 receptor occupancy. Therapy with antihistamines can be better guided by considering histamine H_1 receptor occupancy from the view of their sedative properties.

Keywords: brain, H_1 antihistamines, histamine H_1 receptors, histamine neurons, PET, receptor occupancy, sedation, tissue pharmacokinetics

Expert Opin. Drug Saf. [Early Online]

1. Physiological functions of neuronal histamine

Histamine is involved in a wide variety of physiological functions such as smooth muscle contraction, vascular permeability, gastric secretion, neurotransmission and eosinophil functions, all of which are manifested via four types of receptors, namely, the H_1, H_2, H_3 or H_4 receptors. Histamine is localized mainly in mast cells, enterochromaffin-like cells and neurons among other cells. The neuronal localization of histamine had long been unknown. In 1984, Watanabe *et al.* discovered the localization of the histaminergic neuron system in the posterior hypothalamus (**Figure 1**). Notably, histamine has both excitatory and inhibitory functions [1], as shown in **Table 1**. The excitatory functions involve an increase in wakefulness, augmentation of learning and memory, increase in locomotor activity and augmentation of pain reception. The inhibitory functions involve feeding behaviors, stress-induced excitation or convulsion, development of stimulant psychosis and inhibition of denervation-induced supersensitivity. Histamine neurons via the H_1 and H_2 receptors play an important role in the sleep–wake mechanism, one of the important activation mechanisms of cerebral cortex functions [1,2]. The administration of antihistamines with high brain penetrability, therefore, interferes with the above-mentioned mechanisms, resulting in the reduction of wakefulness, decrease in learning and memory, and induction of obesity and convulsion.

10.1517/14740338.2011.562889 © 2011 Informa UK, Ltd. ISSN 1474-0338

Article highlights.

- Histamine neurons play an important role in the activation of cerebral cortex functions via the H_1 and H_2 receptors.
- H_1 antihistamines sometimes have considerable sedative effects as a drawback owing to their ease of penetration across the BBB.
- Binding affinities for H_1 receptors (potency) vary considerably among H_1 antihistamines, although the clinical efficacies (E_{max}) are similar.
- A large difference lies in their sedative effects, although the sedating properties of H_1 antihistamines are not proportional to their potency.
- The molecular positron emission tomography studies reveal that the sedative properties of H_1 antihistamines are proportional to the H_1 receptor occupancy.
- Recommended therapy with non-sedating H_1 antihistamines can be better guided by considering histamine H_1 receptor occupancy.

This box summarizes key points contained in the article.

2. Pharmacology of antihistamines

Antihistamines were developed by Daniel Bovet, an Italian pharmacologist, in 1937. These antihistamines also served as a prototype of drugs acting on the CNS, such as antipsychotics or antidepressants. In 1957, Bovet was awarded a Nobel Prize in Physiology and Medicine for these and other contributions in pharmacology. Although effective for allergic diseases, first generation antihistamines have potent sedative effects as a drawback owing to their ease of penetration across the BBB. Moreover, their selectivity toward H_1 receptors is low, causing frequent adverse reactions such as dry mouth, urinary retention and tachycardia due to anticholinergic activity. To overcome these drawbacks, second generation antihistamines with high H_1 receptor selectivity, low brain permeability and long plasma half-lifes have been developed. In second generation, non-sedative antihistamines, hydrophilic functional groups (-COOH, $-NH_2$) are introduced in order to reduce their BBB permeability as a way of decreasing their sedative effects (**Figure 2**). Those having a carboxy group (-COOH), among other groups, are used worldwide as non-sedative antihistamines (**Figure 2**). In particular, ebastine and loratadine are prodrugs that pose pharmacological problems unless adequately converted into their active carboxy or amino forms in the body. Because loratadine is metabolized by CYP3A4 and CYP2D6, which are susceptible to drug interactions, its active metabolite, desloratadine, is usually used in Europe and the US. Cetrizine is a mixture of (*R*) and (*S*) optical isomers; the (*R*) isomer levocetrizine is used in most of countries as the first-line treatment. Bepotastine, which has a similar profile to cetrizine and was developed in Japan, is an optically single compound.

Binding affinities for H_1 receptors vary considerably among antihistamines. Antidepressants and some antipsychotics bind to H_1 receptors more strongly than classical antihistamines, with potency differences of 200 times or more. Specifically, the tricyclic antidepressant doxepin is the most potent H_1 antagonist. [^{11}C]-labeled doxepin was used in our positron emission tomography (PET) studies because it has the highest binding affinity. Olopatadine is a potent, non-sedative, second generation antihistamine that has a structure similar to that of doxepin, as well as reduced brain penetrability owing to the introduction of a carboxy group [3]. The binding affinities (K_i values) of non-sedative, second generation antihistamines for histamine H_1 receptors are summarized from the references in **Table 2** [3-5]. Based on the large difference in potency of their binding affinities, second generation antihistamines can be classified into three groups: low potency group (loratadine and fexofenadine), intermediate potency group (cetrizine, bepotastine and olopatadine) and high potency group (levocetirizine, desloratadine and epinastine). However, the efficacies of these antihistamines as expressed by the maximum reaction (E_{max}) are nearly the same despite the differences in the potency.

3. Sedative effects of antihistamines

A big difference other than potency among antihistamines lies in their sedative effects, although the sedating properties of antihistamines are not proportional to their potency. It is well known that ingestion of first generation antihistamines markedly decreases work or learning efficiency. First generation antihistamines may cause serious accidents because of recognition or judgment errors if taken before operating large machines with potential risks, driving cars or flying airplanes. The sedative effects of antihistamines are induced when these drugs penetrate the brain and block signal transmission via the histaminergic neuron system. Neuronal histamine activates the cerebral cortex via histamine H_1 receptors (**Figure 1**) localized abundantly in the frontal cortex and cingulate gyrus in the brain [6]; antihistamines that have penetrated the brain lower cognitive function by inhibiting the activation of the cerebral cortex. The sedative effects of antihistamines are closely associated with brain penetrability or BBB permeability. Most second generation antihistamines are hydrophilic owing to their carboxy group; in addition, they are substrates for P-glycoprotein, which functions as a drug efflux pump.

The sedative effects of antihistamines include sleepiness and impaired performance. There are two aspects of emotion, emotional experience and emotional expression; it is not scientific to assess the sedative effects of antihistamines by sleepiness alone. There are many tests for assessing cognitive function to objectively measure such sedative effects [7-9]. With the aid of computer programs, we have used visual reaction tasks or car driving simulation tasks [10-12], or indoor or outdoor car driving tests [13] to measure reaction times or correct response. Subjective sleepiness can be obtained by hearing from the subjects using the Stanford Sleepiness Scale or Line Analog Rating Scale. There were more than a

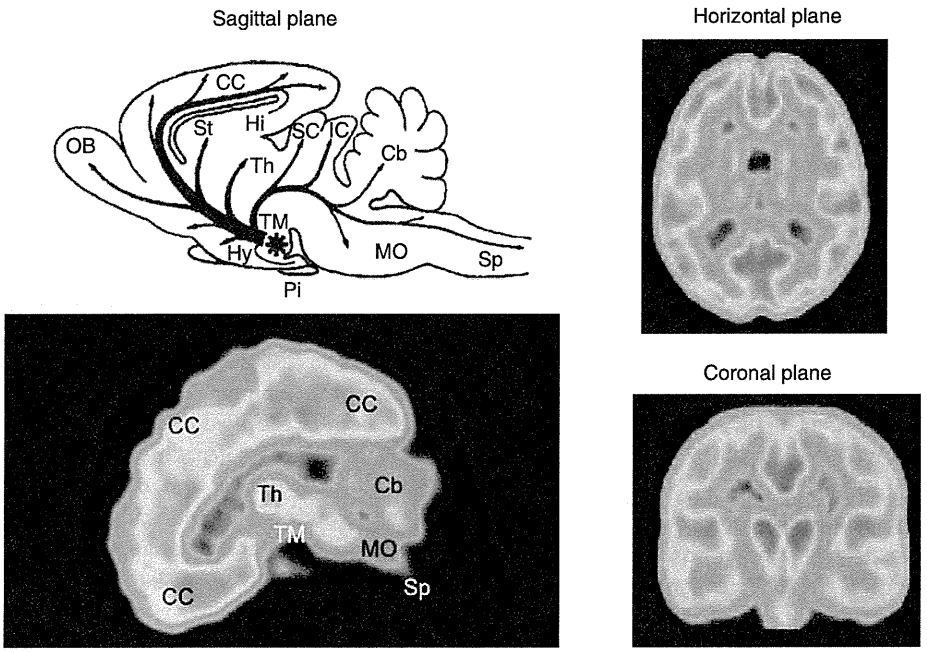

Figure 1. Distributions of the histamine neuron system and brain H_1 receptors visualized by PET. The distribution of the histamine neuron system in the rat brain is shown (upper left). Histamine neurons are located in the tuberomammillary nucleus of posterior hypothalamus (star in the figure), and their nerve fibers are distributed throughout the brain. Released neuronal histamine transmits stimuli via the H_1 and H_2 receptors located on the postsynaptic membrane. The distributions of histamine H_1 receptors in the human brain as measured by [^{11}C] doxepin are shown: sagittal plane (lower left), horizontal plane (upper right) and coronal plane (lower right). H_1 receptors are densely located in the cingulate gyrus, frontal lobe and temporal lobe. Because the specific binding in the cerebellum is scarce, it is used as a reference region in the PET analysis.
Cb: Cerebellum; CC: Cerebral cortex; Hi: Hippocampus; Hy: hypothalamus; IC: Inferior colliculus; MO: Medulla oblongata; OB: Olfactory bulb; PET: Positron emission tomography; Pi: Pituitary gland; SC: Superior colliculus; Sp: Spinal cord; St: Striatum; TM: Tuberomammillary (nucleus of origin of histamine neuron); Th: Thalamus.

Table 1. Functional roles of the histaminergic neuron system.

Functions	Overall functions of histamine neurons
Excitatory functions	
Sleep–wake cycle	Maintenance of wakefulness
	Increase in locomotor activity
Cognition	Augmented learning and memory
Energy metabolism	Induction of brain glycogen hydrolysis
Inhibitory functions	
Feeding	Inhibition of feeding behavior
Convulsion	Inhibition of convulsion
Stress	Inhibition of stress-induced excitation
MAP-induced psychosis	Inhibition of kindling formation
Neural plasticity	Inhibition of denervation-induced supersensitivity

few cases where the percentages of correctly answered questions were nearly zero among patients who had answered that they never felt subjective sleepiness. There were cases where subjective sleepiness and impaired performance do not coincide; therefore, the importance of objectively assessed impaired performance is assured. In cognitive function studies of newer second generation antihistamines, comparison among three groups (i.e., a group with sedative antihistamine as an active control, a placebo group and a test drug group) is necessary. An active control group is necessary in that if there were no significant differences between the placebo and active control groups, the study results cannot be evaluated, indicating that the sensitivity of the measurement method is insufficient [14].

4. Histamine H_1 receptor occupancy in the brain

The use of PET enables the observation of different behaviors of biological molecules such as neuroreceptors and transporters non-invasively from outside the body and, therefore, it is widely used in drug discovery and development processes and evaluations of treatment efficacy. We have developed a method of measuring histamine H_1 receptors using [^{11}C] pyrilamine and [^{11}C] doxepin, and have used this method in human pharmacological studies [15,16]. To verify the specific binding of [^{11}C]doxepin to H_1 receptors, the

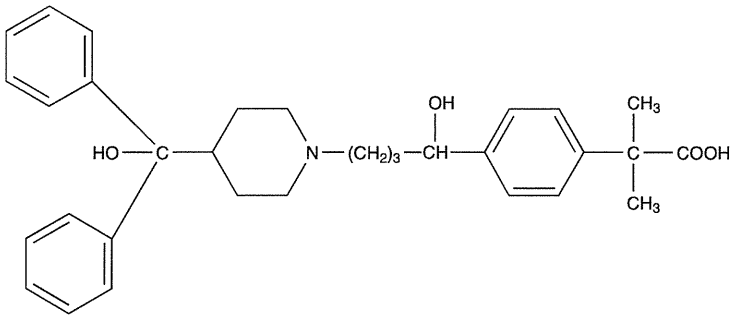

(R)(S) Fexofenadine

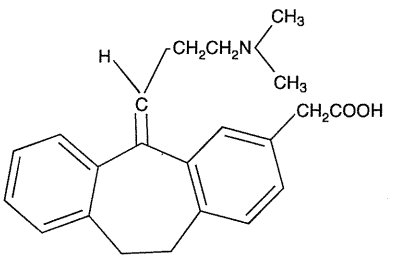

(Z) Olopatadine

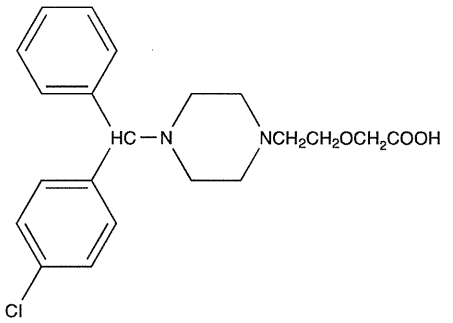

(R)(S) Cetirizine
(R) Levocetirizine

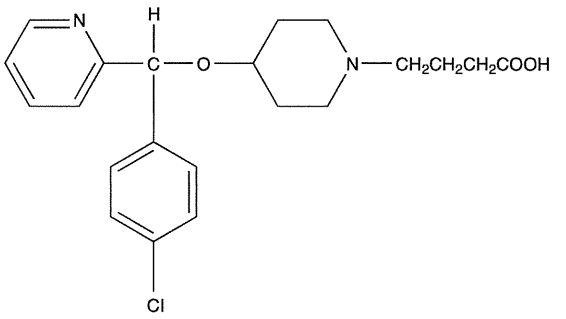

(S) Bepotastine

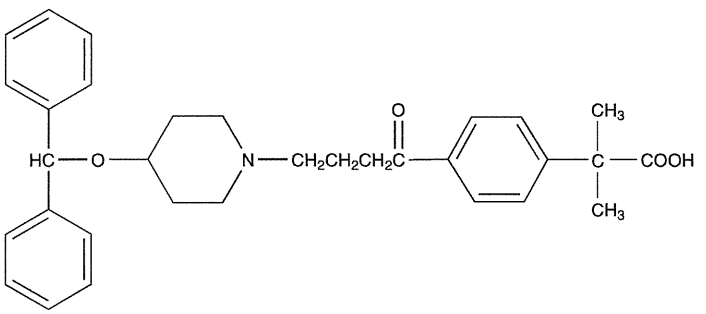

Carebastine
(Active metabolite of ebastine)

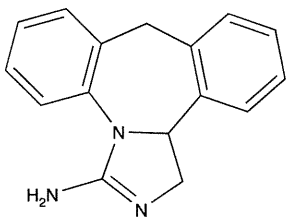

(R)(S) Epinastine

Figure 2. Non-sedative, second generation antihistamines with carboxy and/or amino group(s). The newer antihistamines listed can be prescribed as oral routes of administration in Japan.

characteristics of the binding of doxepin to brain tissues were examined using histamine H_1 receptors gene knockout mice. Doxepin has two saturable binding sites with high and low affinities in the wild-type mice. However, only negligible labeling of doxepin was observed in H1R null mice in a condition with low receptor occupancy. These data demonstrate clearly that the high affinity component of doxepin binding is associated with H_1 receptors.

We have also developed a method of objectively evaluating the sedative effects of antihistamines following ingestion using H_1 receptor occupancy in the brain, which is obtained by measuring H_1 receptors using [^{11}C] doxepin [17].

Table 2. Binding affinities of second generation non-sedating antihistamines for H_1 receptors.

H_1 receptor antagonist	K_i (nmol/l)
Levocetirizine	3*
Desloratadine	3
Epinastine	4.5
Levocabastine	19
Olopatadine	34
Bepotastine	34‡
Cetirizine	101
Fexofenadine	218
Loratadine	231

This table shows the binding affinities (K_i values) of representative second generation antihistamines with carboxy and/or amino group(s) from the [^{3}H] pyrilamine binding to H_1 receptors expressed on CHO cells with human H_1 receptors [3]. The lower the K_i values the stronger the binding for H_1 receptors. Note that the binding affinities of the second generation antihistamines (i.e., potency) vary considerably.
*The K_i of levocetirizine is from a separate report of similar [^{3}H]pyrilamine binding experiments using CHO cells expressed with human H_1 receptors [4].
‡The K_i of bepotastine is from the classical [^{3}H]pyrilamine binding to the guinea-pig brain homogenate [5].
CHO: Chinese hamster ovary.

[^{11}C] doxepin is intravenously administered at t_{max} after the oral administration of an antihistamine, and H_1 receptor density is non-invasively measured by PET, followed by the measurement of receptor occupancy as compared to the values measured when the placebo was administered [18-23]. Usually, comparison is made among three groups, that is, a placebo group, test drug group and sedative antihistamine group. However, unlike cognitive function, receptor occupancy is an absolute value, and it is sufficient to use two groups, namely, a placebo group and test drug group. In addition, it is possible to compare receptor occupancy among different studies. Although continuous PET measurement in the brain for about 90 min and the blood radioactivity (total radioactivity minus that of metabolites) by blood sampling are necessary for an accurate model analysis of receptors, we have thus far simplified the method by shortening the PET scanning time and reducing the number of blood sampling [24-26].

When the penetration level of a pre-administered antihistamine in the brain is high as observed in the case of diphenhydramine, most of the H_1 receptors are blocked. Therefore, the binding state of [^{11}C] doxepin distributed in the brain is affected (**Figure 3**). H_1 receptor occupancies of antihistamines used in the clinic have been measured by researchers mainly from Tohoku University and also from other institutions (**Figure 4**) [6]. The results confirmed that classical antihistamines which are more likely to induce sedative effects occupy more H_1 receptors in the brain. A study in which receptor occupancy measurements and cognitive function tests were performed simultaneously revealed that impaired performance was definitely caused when the H_1 receptor occupancy was 50% or higher [10]. On the other hand, the H_1 receptor occupancies of recently developed, low brain-penetrating, newer second generation antihistamines are as low as 30% or less. In particular, the receptor occupancies of epinastine, ebastine, loratadine, terfenadine and fexofenadine, characterized as having weak sedative effects, are especially low. As for antihistamines with H_1 receptor occupancies of 20% or less, impaired performance is almost impossible to detect in cognitive function tests [20,23].

The current classifications of antihistamines as 'first generation' and 'second generation' are based on the time of development; therefore, some sedative antihistamines may be classified as second generation drugs depending on the time of development. It is possible that antihistamines are sold as non-sedative drugs claiming that no significant differences between the drug and the placebo exist; however, it is possible that the results had been based on cognitive function tests of insufficient sensitivity or sleepiness alone. To classify antihistamines according to their sedative effects, we have proposed the use of H_1 receptor occupancy and, therefore, classify antihistamines into three groups: a sedative group (antihistamines with H_1 receptor occupancy higher than 50%), a less sedative group (antihistamines with H_1 receptor occupancy between 20 and 50%) and a non-sedative group (antihistamines with H_1 receptor occupancy of 20% or lower) [6,14].

Shamsi and Hindmarch and McDonald *et al.* analyzed all reports in the literature of randomized, placebo-controlled, double-blind trials and calculated the incidence rates of the sedative effects of various antihistamines in terms of subjective and objective aspects [27,28]. The incident rates of sedation obtained were closely correlated with the results of H_1 receptor occupancy as measured by PET as shown in the inset of **Figure 4**.

The first generation antihistamines are profoundly sedative and impair CNS function at virtually all doses tested, due to their ease of passage across the BBB. Several second generation antihistamines also cross the BBB, but their effects on performance are much less marked than those of the first generation drugs. There may be dose-related impairments of CNS function, as the effects are more pronounced with increasing doses of some second generation antihistamines (**Figure 5**). Thus, when any impairment of CNS function is demonstrated for a particular second generation drug, it can be classified only as a 'relatively non-sedative' or 'less sedative' drug, but not a 'non-sedative' drug. However, several second generation drugs do not penetrate the BBB with the increment of doses and are, therefore, truly non-sedative, that is, not passing into the CNS and having no significant effects on CNS function in daily life, even when used at doses in excess of those commonly recommended.

5. Guidelines for antihistamine use and H_1 receptor occupancy

Although the proper use of antihistamines with early onset of allergic action is becoming important as the number of

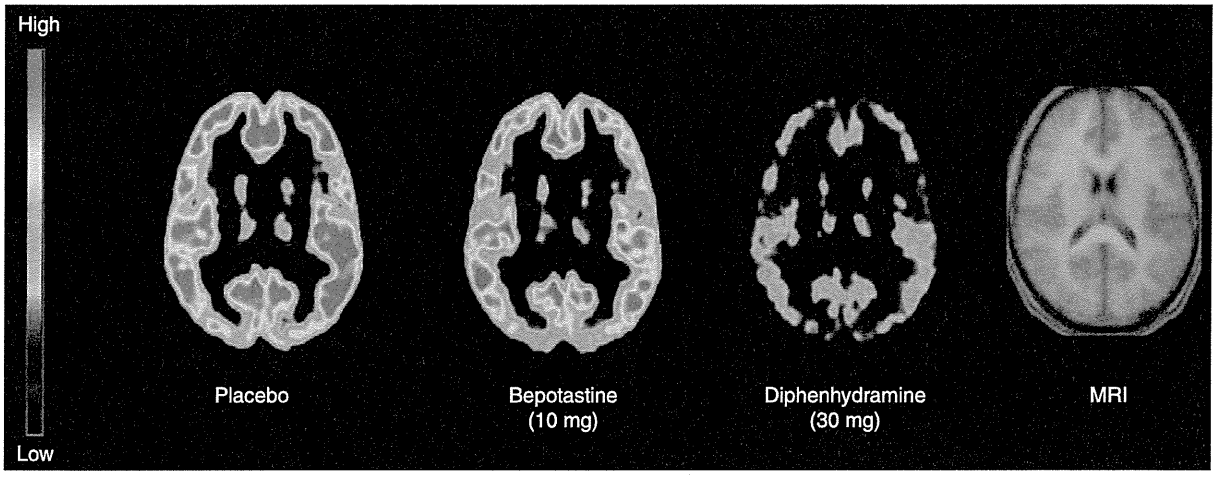

Figure 3. H_1 receptors after ingestion of bepotastine and diphenhydramine. The binding abilities of H_1 receptors were measured after oral administration of a placebo, the second generation antihistamine bepotastine (10 mg) or the first generation antihistamine diphenhydramine (30 mg). H_1 receptor binding ability was decreased by ~ 14% after the bepotastine administration compared with the placebo administration. On the other hand, receptor binding ability was decreased by > 50% after the diphenhydramine administration.

patients with allergy is increasing, sufficient consensus as to the ideal antihistamines has not yet been reached. Under these circumstances, an expert meeting called Consensus Group of New Generation of Antihistamines (CONGA) was organized, who proposed a standard for ideal antihistamines and adopted a classification regarding the sedative effects of antihistamines based on their H_1 receptor occupancy [14]. Regarding newer second generation antihistamines with low brain penetrability, the CONGA standard specifically describes that 'non-sedative' properties should be confirmed by H_1 receptor occupancy.

H_1 antihistamines are recommended for treatment of allergic disease in many major guidelines. In the treatment of allergic rhinitis, the guidelines in Europe and the US place second generation anti-histamines as first-line treatment and first generation antihistamines as 'not recommended' [29]. In the treatment of urticaria, the guidelines in Europe recommend non-sedating anti-histamines as first-line treatment [30]. In addition, the guidelines recently published for management of atopic dermatitis of the Japanese Dermatological Association (downloadable free of charge from http://www.dermatol.or.jp/) clarified the criteria for 'non-sedative antihistamines' for the first time as Japanese guidelines and has adopted the classification based on H_1 receptor occupancy. Interestingly, a Global Allergy and Asthma European Network (GA^2LEN) raised the issue of better consumer protection by recommending that first generation sedating H_1 antihistamines should no longer be available over-the-counter as prescription-free drugs for self-medication of allergic and other diseases because both accidental and intentional deaths have occurred [31].

6. Future perspectives: hangover and multiple dosing

We have been conducting studies on measurement of histamine H_1 receptor occupancy at t_{max} after a single administration of antihistamines. Although we currently have plasma pharmacokinetic models, we still do not have tissue pharmacokinetic models. Therefore, receptor occupancy must be measured at several time points after a single administration. Measurements of brain penetration and elimination half-lifes in the brain during repeated dosing are needed. Furthermore, measurements of brain penetration after topical administration and applications for allergy patients [32] as well as for genetic polymorphism are important subjects for the future.

We recently demonstrated that the next-day residual sedative effect after night-time administration of the OTC sleep aid diphenhydramine was verified for the first time by direct PET measurement of H1RO [33]. At night, first generation H_1 antihistamines increase the latency to the onset of rapid eye movement (REM) sleep and reduce the duration of REM sleep [34]. Furthermore, residual effects, or hang-over, are still present the next morning. Such effects include impairment in divided attention, vigilance, working memory and sensory-motor performance, and reduced latency to daytime sleep without subjectively reported somnolence.

7. Expert opinion

Antihistamines are generally used for relieving allergy symptoms as the first-line treatment. Antihistamines are

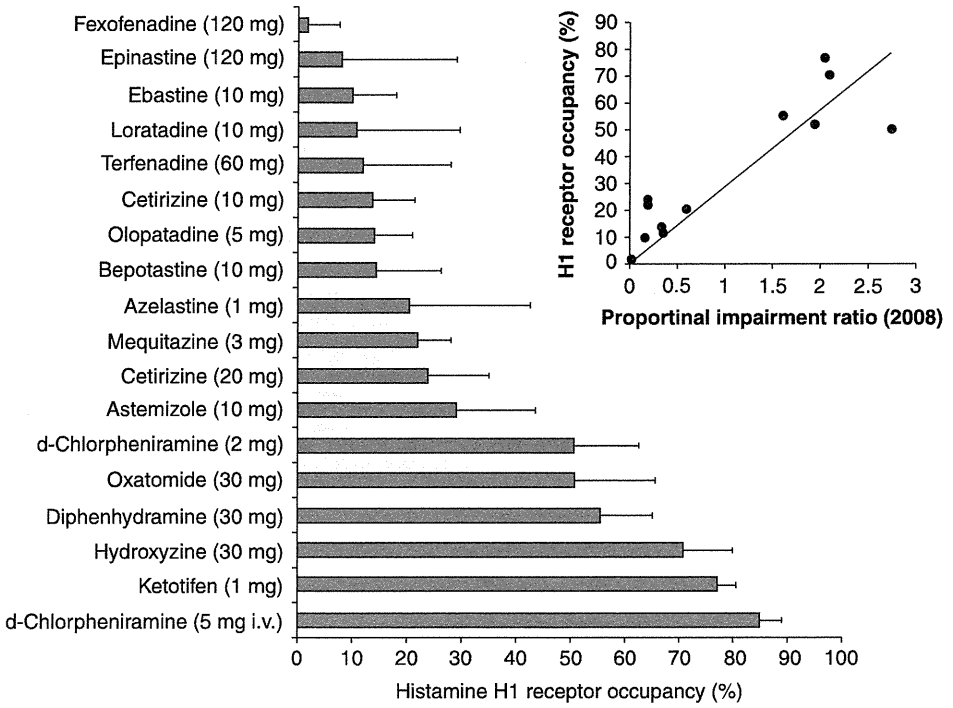

Figure 4. H_1 receptor occupancies of antihistamines marketed in Japan. This is a summary of our ongoing measurements of H_1 receptor occupancies after antihistamine administration using [^{11}C] doxepin-PET. The H_1 receptor occupancy by antihistamines is proportional to their sedative effects. Note that H_1 receptor occupancies vary considerably even among second generation antihistamines. With regard to the ideal standard of antihistamines, an expert meeting body called the Consensus Group of New Generation of Antihistamines or CONGA was organized, and a standard based on consensus on ideal, newer generation antihistamines was formulated. In this standard, evaluation of sedative effects using PET is recommended. Antihistamines are classified into three groups: a non-sedative group (H_1 receptor occupancy, 20% or lower), a less sedative group (H_1 receptor occupancy, between 20 and 50%) and a sedative group (H_1 receptor occupancy, higher than 50%). The distinction between non-sedative and less sedative drugs is not very clear. Receptor occupancy (%) is calculated using the following equation:

$$\left[1-\frac{(\text{H1R binding at Tmax after taking an antihistamine})}{\text{H1R binding after taking a placebo}}\right]\times 100\%$$

Inset: Correlation between histamine H_1 receptor occupancy and proportional impairment ratios from the literature of randomized, placebo-controlled, double-blind trials.

generally very safe drugs judging from the studies using histamine H_1 receptor genes knockout mice [18]; however, the most troublesome effects in humans are the potent sedation when their brain penetration level is high. Although second generation antihistamines which have low brain penetrability have been developed, comparison of their differences in sedative effects only by subjective sleepiness or cognitive function tests is difficult. In particular, PET is frequently used not only for disease diagnosis in the clinic but also for molecular imaging studies related to drug discovery and the clinical development. Molecular imaging of histamine H_1 receptors by PET has been developed, and the use of antihistamine occupancy of H_1 receptors in the brain recommended as an objective and absolute index of sedative effects.

Acknowledgments

The authors thank Drs R Iwata, Y Funaki, K Hiraoka and S Furumoto for performing molecular PET studies.

Declaration of interest

This work was supported in part by Grants-in-Aid for Scientific Research from the Japan Society for Promotion of Science (JSPS) as well as by grants from the Japan Society for Technology (JST) on research and education in "molecular imaging" and Industrial Technology Development organization (NEDO) on research in "microdose clinical studies". In the last 5 years, K Yanai and M Tashiro have received unrestricted

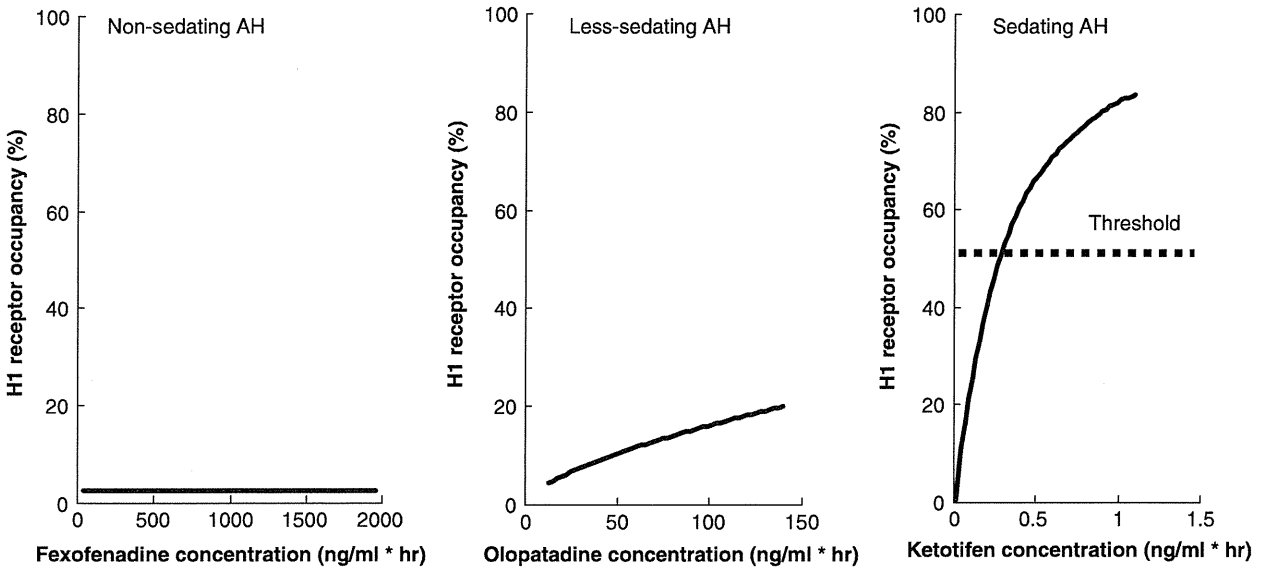

Figure 5. Relationship between histamine H_1 receptor occupancy and drug concentration in plasma. Antihistamines can be classified into non-sedative, less sedative and sedative groups based on the H_1 receptor occupancy and mean plasma concentration of the drugs measured during positron emission tomography. The H_1 receptor occupancies of non-sedative antihistamines (fexofenadine, ebastine and terfenadine) are not correlated to the plasma concentrations of the drugs. The H_1 receptor occupancies of less sedative antihistamines (bepotastine, cetrizine and olopatadine) are proportional to some degree to the plasma concentrations of the drugs and have increased brain penetration. When administered, the sedative antihistamines such as chlorpheniramine, hydroxyzine and ketotifen rapidly penetrate the brain.

research grants support and lecture honorarium from manufactures of 2nd generation antihistamines, including Sanofi-aventis, GlaxoSmithKline, Merck, Boehringer-Ingelheim, Kyowa-Kirin, Mitsubishi Tanabe, Dainippon-Sumitomo and Eisai. Other authors have no conflict of interest. Decisions regarding all aspects of the review were made by all members of the study group of Tohoku University without consulting with pharmaceutical companies.

Bibliography

1. Watanabe T, Yanai K. Studies on functional roles of the histaminergic neuron system by using pharmacological agents, knockout mice and positron emission tomography. Tohoku J Exp Med 2001;195:197-217
2. Haas HL, Sergeeva OA, Selbach O. Histamine in the nervous system. Physiol Rev 2008;88:1183-241
3. Matsumoto Y, Funahashi J, Mori K, et al. The noncompetitive antagonism of histamine H1 receptors expressed in Chinese hamster ovary cells by olopatadine hydrochloride: its potency and molecular mechanism. Pharmacology 2008;81:266-74
4. Gillard M, Van Der Perren C, Moguilevsky N, et al. Binding characteristics of cetirizine and levocetirizine to human H1 histamine receptors: contribution of Lys(191) and Thr(194). Mol Pharmacol 2002;61:391-9
5. Kato M, Nishida A, Aga Y, et al. Pharmacokinetic and pharmacodynamic evaluation of central effect of the novel antiallergic agent betotastine besilate. Arzneimittelforschung 1997;47:1116-24
6. Yanai K, Tashiro M. The physiological and pathophysiological roles of neuronal histamine: an insight from human positron emission tomography studies. Pharmacol Ther 2007;113:1-15
7. Weiler JM, Bloomfield JR, Woodworth GG, et al. Effects of fexofenadine, diphenhydramine, and alcohol on driving performance. A randomized, placebo-controlled trial in the Iowa driving simulator. Ann Intern Med 2000;132:354-63
8. Vuurman EF, van Veggel LM, Uiterwijk MM, et al. Seasonal allergic rhinitis and antihistamine effects on children's learning. Ann Allergy 1993;71:121-6
9. Boyle J, Eriksson M, Stanley N, et al. Allergy medication in Japanese volunteers: treatment effect of single doses on nocturnal sleep architecture and next day residual effects. Curr Med Res Opin 2006;22:1343-51
10. Okamura N, Yanai K, Higuchi M, et al. Functional neuroimaging of cognition impaired by a classical antihistamine, d-chlorpheniramine. Br J Pharmacol 2000;129:115-23
11. Tagawa M, Kano M, Okamura N, et al. Differential cognitive effects of ebastine and d-chlorpheniramine in healthy subjects. Br J Clin Pharmacol 2002;53:296-304
12. Mochizuki H, Tashiro M, Tagawa M, et al. The effects of a sedative antihistamine, d-chlorpheniramine, on visuomotor spatial discrimination and regional brain activity as measured by positron emission tomography (PET). Hum Psychopharmacol 2002;17:413-18
13. Tashiro M, Horikawa E, Mochizuki H, et al. Effects of fexofenadine and hydroxyzine on brake reaction time during car-driving with cellular phone use. Hum Psychopharmacol 2005;20:501-9
14. Holgate ST, Canonica GW, Simons F, et al. Consensus group on new-generation antihistamines (CONGA): present status and recommendations. Clin Exp Allergy 2003;33:1305-24
15. Yanai K, Yagi N, Watanabe T, et al. Specific binding of [3H]pyrilamine to histamine H1 receptors in guinea pig brain in vivo: determination of binding parameters by a kinetic four-compartment model. J Neurochem 1990;55:409-20
16. Yanai K, Watanabe T, Yokoyama H, et al. Histamine H1 receptors in human brain visualized in vivo by [11C]doxepin and positron emission tomography. Neurosci Lett 1992;137:145-8
17. Yanai K, Ryu JH, Watanabe T, et al. Histamine H1 receptor occupancy in human brains after single oral doses of histamine H1 antagonists measured by positron emission tomography. Br J Pharmacol 1995;116:1649-55
18. Yanai K, Okamura N, Tagawa M, et al. New findings in pharmacological effects induced by antihistamines: from PET studies to knock-out mice. Clin Exp Allergy 1999;29(Suppl 3):29-36
19. Tagawa M, Kano M, Okamura N, et al. Neuroimaging of histamine H1-receptor occupancy in human brain by positron emission tomography (PET): a comparative study of ebastine, a second-generation antihistamine, and (+)-chlorpheniramine, a classical antihistamine. Br J Clin Pharmacol 2001;52:501-9
20. Tashiro M, Sakurada Y, Iwabuchi K, et al. Central effects of fexofenadine and cetirizine: measurement of psychomotor performance, subjective sleepiness, and brain histamine H1-receptor occupancy using [11C] doxepin positron emission tomography. J Clin Pharmacol 2004;44:890-900
21. Tashiro M, Mochizuki H, Sakurada Y, et al. Brain histamine H receptor occupancy of orally administered antihistamines measured by positron emission tomography with [11C] doxepin in a placebo-controlled crossover study design in healthy subjects: a comparison of olopatadine and ketotifen. Br J Clin Pharmacol 2006;61:16-26
22. Tashiro M, Duan X, Kato M, et al. Brain histamine H1 receptor occupancy of orally administered antihistamines, bepotastine and diphenhydramine, measured by PET with [11C]doxepin. Br J Clin Pharmacol 2008;65:811-21
23. Tashiro M, Kato M, Miyake M, et al. Dose dependency of brain histamine H1 receptor occupancy following oral administration of cetirizine hydrochloride measured using PET with [11C]doxepin. Hum Psychopharmacol 2009;24:540-8
24. Mochizuki H, Kimura Y, Ishii K, et al. Quantitative measurement of histamine H1 receptors in human brains by PET and [11C]doxepin. Nucl Med Biol 2004;31:165-71
25. Mochizuki H, Kimura Y, Ishii K, et al. Simplified PET measurement for evaluating histamine H1 receptors in human brains using [11C]doxepin. Nucl Med Biol 2004;31:1005-11
26. Suzuki A, Tashiro M, Kimura Y, et al. Use of reference tissue models for quantification of histamine H1 receptors in human brain by using positron

emission tomography and [11C]doxepin. Ann Nucl Med 2005;19:425-33

27. Shamsi Z, Hindmarch I. Sedation and antihistamines: a review of inter-drug differences using proportional impairment ratios. Hum Psychopharmacol 2000;15(S1):S3-S30

28. McDonald K, Trick L, Boyle J. Sedation and antihistamines: an update. Review of inter-drug differences using proportional impairment ratios. Hum Psychopharmacol 2008;23:555-70

29. Plaut M, Valentine MD. Clinical practice. Allergic rhinitis. N Engl J Med 2005;353:1934-44

30. Zuberbier T, Asero R, Bindslev-Jensen C, et al. EAACI/GA2LEN/EDF/WAO guideline: management of Urticaria. Allergy 2009;64:1427-43

31. Church MK, Maurer M, Simons FER, et al. Risk of first-generation H1-antihistamines: a GA2LEN position paper. Allergy 2010;65:459-66

32. Senda M, Kubo N, Adachi K, et al. Potential measured with PET under a test dose of olopatadine, an antihistamine, is reduced after repeated administration of olopatadine. J Nucl Med 2009;50:887-92

33. Zhang D, Tashiro M, Shibuya K, et al. Next-day residual sedative effect after nighttime administration of an over-the-counter antihistamine sleep aid, diphenhydramine, measured by positron emission tomography. J Clin Psychopharmacol 2010;30:694-701

34. Boyle J, Eriksson M, Stanley N, et al. Allergy medication in Japanese volunteers: treatment effect of single doses on nocturnal sleep architecture and next day residual effects. Curr Med Res Opin 2006;22:1343-51

Affiliation

Kazuhiko Yanai[†1,2,3] MD PhD,
Dongying Zhang[1], Manabu Tashiro[2],
Takeo Yoshikawa[1], Fumito Naganuma[1],
Ryuichi Harada[1], Tadaho Nakamura[1],
Katsuhiko Shibuya[1] & Nobuyuki Okamura[1]
[†]Author for correspondence
[1]Tohoku University Graduate School of Medicine,
Department of Pharmacology,
2-1 Seiryo-machi, Aoba-ku,
Sendai 980 8575, Japan
[2]Tohoku University,
Cyclotron and Radiosiotope Center,
Division of Nuclear Medicine,
6-3 Aoba, Aramaki,
Aoba-ku, Sendai 980 8578, Japan
[3]Professor,
Tohoku University
Graduate School of Medicine,
Department of Pharmacology,
2-1 Seiryo-machi, Aoba-ku,
Sendai 980 8575, Japan
Tel: +81 22 717 8055; Fax: +81 22 717 8060;
E-mail: yanai@med.tohoku.ac.jp

TISSUE ENGINEERING: Part A
Volume 18, Numbers 5 and 6, 2012

DOI: 10.1089/ten.tea.2011.0349

Granule Size–Dependent Bone Regenerative Capacity of Octacalcium Phosphate in Collagen Matrix

Yuji Tanuma, D.D.S., Ph.D.,[1,2,*] Takahisa Anada, Ph.D.,[2,*] Yoshitomo Honda, D.D.S., Ph.D.,[2]
Tadashi Kawai, D.D.S., Ph.D.,[1] Shinji Kamakura, D.D.S., Ph.D.,[3]
Seishi Echigo, D.D.S., Ph.D.,[1] and Osamu Suzuki, Ph.D.[2]

The present study was designed to determine whether the osteoconductivity of octacalcium phosphate–collagen (OCP/Col) composite can be improved by controlling the granule size of OCP. The granules of synthetic OCP, with diameters in the range of 53 to 300, 300 to 500, and 500 to 1000 μm, were used as an inorganic source of composite materials mixed with atelo-Col. After vacuum dehydrothemal treatment, OCP/Col disks were implanted into critical-sized calvaria defects in Wistar rats for 4, 8, and 12 weeks and examined radiographically, histologically, histomorphometrically, and histochemically. The materials were characterized according to mercury intrusion porosimetry and scanning electron microscopy. X-ray diffraction was performed before and after implantation. The dissolution of OCP crystals in a Col matrix was determined by immersing OCP/Col disks in a culture medium. OCP/Col had a constant pore size (~30 μm) regardless of OCP granule size. OCP in the Col matrix tended to convert to hydroxyapatite (HA) during the implantation. OCP/Col with the smallest granules of OCP enhances both bone regeneration and biodegradation the most through tartrate-resistant acid phosphatase (TRAP)-positive osteoclastic cellular resorption of OCP granules. The smallest OCP granules in the Col matrix showed the highest dissolution and had the greatest potential to form HA. The results indicated that the size of the included OCP granules can controll the osteoconductivity of OCP/Col. The overall results suggest that the physicochemical property of OCP crystals is a factor that determines the bone regenerative capacity of OCP/Col in critical-sized calvaria large bone defects in rats.

Introduction

One of the characteristics of biomaterials used at load-bearing sites as a nonresorbable synthetic bone substitute is high strength,[1] although there is consensus that bone substitute materials should provide a framework for continuous bone resorption and bone deposition[2] because such biodegradable materials are integrated into a natural bone remodeling process caused by the resorption of the existing bone matrix together with the implanted materials by osteoclasts and the deposition of new bone matrix by osteoblasts.[2] Much attention has been given to the investigation and development of various biodegradable calcium phosphate ceramics *in vivo*, such as beta-tricalcium phosphate (β-TCP),[3,4] with an adjusted level of bioactivity and the capacity for new bone formation, but no ideal material condition has yet been found.

The solubility of calcium phosphates is a factor affecting their possible order of dissolving in physiological environments.[5] β-TCP is more soluble than hydroxyapatite (HA) in a neutral condition.[5,6] HA has the least solubility of calcium phosphates in that condition and is nonresorbable *in vivo* if it is sintered and has a stoichiometric formula with a calcium:phosphate (Ca/P) molar ratio of 1.67,[3,7] but the stability of HA decreases if a carbonate ion is included in its structure.[8] The physicochemical properties of HA and β-TCP (porosity, shape, and size), which could be associated with the apparent solubility of these materials, have been found to influence the outcome of *de novo* bone formation in bone defects.[9,10] Osteoclast-like cells resorb β-TCP,[4, 10] carbonate-containing HA,[11] and HA with nanoscale[12] *in vivo*, facilitating bone regeneration by these materials in bone defects.

Octacalcium phosphate (OCP), thought to be a precursor to HA[13] that is biodegradable *in vivo*,[14,15] is more soluble than β-TCP in neutral solutions.[5] It was recently found that OCP is capable of inducing osteoclast formation from the co-culturing of osteoblasts and bone marrow cells, through the increase of expression of osteoblasts of osteoclast-inducing

Divisions of [1]Oral Surgery, [2]Craniofacial Function Engineering, Graduate School of Dentistry, Tohoku University, Sendai, Japan.
[3]Division of Bone Regenerative Engineering Laboratory, Graduate School of Biomedical Engineering, Tohoku University.
*These authors contributed equally to this work.

factor RANKL, even in the absence of vitamin D_3, a regulator of osteoclastogenesis.[16] Furthermore, OCP enhances osteoblast differentiation *in vitro*.[17-19] Our previous study showed that OCP, if synthesized under specific conditions, is not only more resorbable than sintered β-TCP in bone defects, because of osteoclastic cellular resorption, but is also more osteoconductive than β-TCP or stoichiometric and nonstoichiometric HA.[20-22] The osteoconductive and biodegradable characteristics of OCP have also been reproduced in the form of a composite with natural polymers, such as Col[23] and alginate.[24] From these findings, we hypothesized that OCP could be used as a source material for various scaffold materials, such as polymers used in tissue engineering, making it possible to include OCP in the bone remodeling process.

There is general consensus that the type of scaffold materials,[25] composition (inorganic versus organic),[26] biodegradability, cell-adhesive property,[25] pore size, and porosity[27] control the bone regenerative property of the materials, including calcium phosphate materials. Bone regeneration has been demonstrated to be enhanced with increasing the granule size of OCP, which is accompanied by the augmented appearance of the osteoclasts around them.[28] The effects of OCP mixing with Col[23] and the dose[29] in the form of granules of OCP in the Col sponge have been examined, but the effect of the size of OCP granules in a Col matrix has not been examined. In this study, we investigated the granule size of OCP and how it affects the bone regenerative and biodegradable properties of the OCP/Col composites in critical-sized rat calvaria bone defects, if the composites are prepared under a constant condition, which ensures that the composite property is relatively constant except for the granule size of OCP.

Materials and Methods

Preparation of OCP, Col disks, and OCP/Col disks

OCP was prepared by mixing calcium and phosphate solutions as described previously.[22] The granules, consisting of an OCP crystal aggregate, were prepared from OCP precipitates by passing through a standard testing sieve. Granules with diameters ranging from 53 to 300 μm, 300 to 500 μm, and 500 to 1,000 μm were used. The sieved OCP granules were sterilized by heating at 120°C for 2 hours. As shown previously, such heating does not affect the physical properties, such as the crystalline structure or specific surface area of OCP granules,[30,31] although it has been reported that temperatures greater than 100°C induce a gradual collapse of the OCP structure due to dehydration.[32,33] A 1% solution of Col was purchased from NMP Collagen PS (Nippon Meat Packers, Tsukuba, Ibaraki, Japan). The solution was adjusted to pH 7.4 to form a gel of Col fibrils. The Col solution was then condensed by centrifugation. The Col suspension at a concentration of 3% was prepared from the condensed Col suspension. OCP granules were added to the concentrated Col and mixed. The weight percentage of OCP in OCP/Col was 77%. This OCP/Col mixture was then lyophilized, and the disks were molded (9-mm diameter, 1 mm thick). The molded OCP/Col underwent dehydrothermal treatment (DHT; 120°C,150°C, or 180°C, 24 hours) in a vacuum drying oven (DP32, Yamato Scientific, Tokyo, Japan) and was then sterilized using electron beam irradiation (5 kGy). The Col disks as the control material were prepared with identical treatments.

Characterization of OCP/Col disks

OCP/Col disks were characterized using X-ray diffraction (XRD). The XRD patterns were recorded using step scanning at 0.05° intervals from 3.0° to 60.0°, with Cu Kα X-rays on a diffractometer (Mini Flex, Rigaku Electrical Co., Ltd., Tokyo, Japan) at 30 kV, 15 mA. The 2θ range measured included the primary peak (100) of OCP at 4.7°. Joint Committee for Powder Diffraction Standard (JCPDS) number 26-1056A9 for OCP and 9-432 for HA were used to identify their crystalline phases. The porosity was determined according to mercury intrusion porosimetry (PoreMaster60GT, analyzed by KN Lab Analysis, Hyogo, Japan). The morphology of OCP/Col disks was examined using a JEOL analytical scanning electron microscope JSM-6390LA (Tokyo, Japan) operating at an accelerating voltage of 10 kV. Gold sputtering was performed before the observation.

Implantation of OCP/Col or Col in rat calvaria bone defect

Twelve-week-old male Wistar rats (SLC, Hamamatsu, Shizuoka, Japan) were used. The principles of laboratory animal care and national laws were followed. The Animal Research Committee of Tohoku University approved all procedures.

The experimental rats were anesthetized with intraperitoneal sodium pentobarbital (50 mg/kg) supplemented by ether inhalation. A skin incision was made aseptically along the bilateral temporal line and the middle of the forehead, and the dissection was continued to the calvarium. The periosteum of the calvarium was ablated, and a full-thickness standardized trephine defect, 9 mm in diameter, was made in the calvarium under continuous saline buffer irrigation. Extreme care was exercised to avoid injury to the midsagittal blood sinus and dura mater. OCP/Col or Col disks were implanted into the trephine defect. As a negative control, untreated animals were processed in the same way except that nothing was implanted after the defects were created. After the defects were treated, the ablated periosteum was repositioned and the skin sutured. Five rats in each of the OCP/Col-treated, Col-treated, and untreated groups were anesthetized and sacrificed for the tissue fixation at 4, 8, and 12 weeks after implantation as described below.

Radiographic analysis

The rats were anesthetized by intraperitoneal sodium pentobarbital (50 mg/kg), and sacrificed with 4% paraformaldehyde in 0.1M PBS (pH 7.4) by perfusion through the aorta for the tissue fixation. The implants were resected together with the surrounding bones and tissues and kept in the same fixative overnight at 4°C. The specimens were radiographed using a microradiography unit (Softex CMR Unit, Softex, Tokyo, Japan) with X-ray film (FR, Fuji Photo Film, Tokyo, Japan) under standardized conditions (20 kV, 5 mA, 1 minute) under which OCP showed no radiopacity.

Tissue preparation

After the radiographic analyses, the samples were decalcified in 10% ethylenediaminetetraacetic acid in a 0.01M phosphate buffer (pH 7.4) for 2 to 4 weeks at 4°C. The

samples were dehydrated in a graded series of ethanol and embedded in paraffin. The center of the defect was extracted and sectioned coronally at a thickness of 5 μm. The sections were stained with hematoxylin and eosin and tartrate-resistant acid phosphatase (TRAP), and photographs were taken using a photomicroscope (Leica DFC300 FX, Leica Microsystems Japan, Tokyo, Japan).

Quantitative micrograph analysis

Light micrographs of the sections stained with hematoxylin and eosin were used for histomorphometric measurements. Photographs projecting the overall defect were taken of each specimen. The percentage of newly formed bone in the defect (n-Bone%) was calculated as the area of newly formed bone per area of the defect originally created by trephination × 100. Likewise, the percentage of remaining OCP in the defect (r-Imp%) was calculated as the area of remaining OCP per area of the defect originally created by trephination × 100. The n-Bone% and r-Imp% were quantified on a computer using Scion Image public domain software (Scion Corporation, Frederick, MD).

XRD of implanted OCP

The OCP implanted in the rat calvaria was examined for XRD. The OCP/Col implanted for 12 weeks was collected from rat calvarial bone defects of two to four rats using tweezers to exclude as much of the soft tissue around the implanted OCP as possible. The OCP/Col was immediately dipped in PBS and deionized water and then in absolute alcohol to dry. The OCP/Col was ground using a mortar and pestle and examined for powder XRD under the same conditions used for the characterization of OCP as reported above.

Dissolution estimation of OCP/Col disks immersed in a culture medium

The concentration of calcium ions (Ca^{2+}) and inorganic phosphate ions (Pi) in an alpha minimal essential medium (αMEM) was determined quantitatively using Calcium E and Phosphor C tests (Wako Pure Chemical Industries, Osaka, Japan), respectively. Ten milligrams of OCP/Col disks was immersed in 750 μL of αMEM for 3 days at 37°C in a 5% carbon dioxide environment. The supernatants after the immersion were collected for Ca^{2+} and Pi quantitative analyses.

Degree of supersaturation of media after immersing OCP/Col composites

Degree of supersaturation (DS) of αMEM and after immersing OCP/Col composites and Col disks was calculated to estimate the dissolution of OCP granules with respect to OCP, HA, and dicalcium phosphate dihydrate (DCPD) in the media. DS can be expressed by dividing the ionic product by the solubility product in objective calcium phosphate compound and stands for saturation when the value is 1. DS is usually calculated using the analytical results of [Ca], [Mg], [Na], [K], [P], [Cl], and [F] and the pH value in conjunction with the three mass balance equations for [Ca], [P], and [Mg], according to previous reports.[34-36] The calculation also assumed the presence of HCO^{3-} in the fluid. The ion pairs considered were CaH_2PO^{4+}, $CaHPO_4^0$, $MgHPO_4^0$, $CaHCO^{3+}$, and $MgHCO^{3+}$. DS was defined in terms of their mean ionic activity product with respect to OCP, HA, and DCPD. In the present calculation, the concentration of Ca^{2+} and Pi obtained using chemical analyses was used. Ionic strength with 150mM as Na^+ was assumed. pH 7.4 and physiologic partial pressure 1.86% in carbonate were used for the calculation. Other species, such as Mg^{2+} and F^-, were assumed to be approximately 0. The solubility product constants used were 2.63×10^{-60} for HA[37] and 1.05×10^{-47} for OCP.[38]

Statistical analysis

Results were expressed as means±standard deviations (SDs). All cellular experiments were performed at least three times and showed reliable reproducibility. Statistical analysis was performed for all of the cellular and histomorphometric experiments using commercial software (Ekuseru-Toukei 2006, Social Survey Research Information, Tokyo, Japan). One-way analysis of variance (ANOVA) was used to compare the means between groups. If the ANOVA was significant, Tukey's multiple comparison analysis was used as a *post hoc* test.

Results

XRD patterns of OCP/Col, OCP, and Col

We prepared OCP/Col with OCP granules 300 to 500 μm in diameter and processed it with different temperatures of DHT (120°C, 150°C, or 180°C). The peaks diffracted from OCP/Col 120°C, OCP/Col 150°C, OCP/Col 180°C, OCP, and Col are shown in Figure 1. Although XRD patterns obtained in OCP/Col disks contained the characteristic (100) reflection of OCP at 2θ=4.7°, corresponding well with those expected from the OCP structure,[39] they showed the structural changes of OCP. OCP in OCP/Col revealed the partial collapse of the (100) peak with a reduction of the (700) peak around 33.6° due to DHT. OCP/Col had an HA-like XRD pattern but the characteristics of OCP.

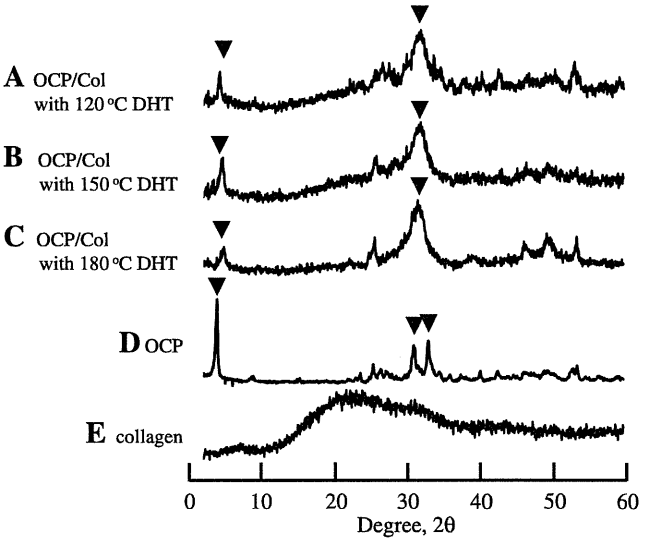

FIG. 1. X-ray diffraction patterns of **(A)** octacalcium phosphate (OCP)/collagen (Col) with 120°C dehydrothermal treatment (DHT), **(B)** OCP/Col with 150°C DHT, **(C)** OCP/Col with 180°C DHT, **(D)** OCP, and **(E)** Col. The size of the OCP granules was 300-500 μm. ▼, OCP reflection.